Investigating Lipid Composition Effects on the Mechanosensitive Channel of Large Conductance (MscL) Using Molecular Dynamics Simulations

Donald E. Elmore and Dennis A. Dougherty
Division of Chemistry and Chemical Engineering, California Institute of Technology, Pasadena, California

ABSTRACT Previous experimental work has shown that the functional properties of the mechanosensitive channel of large conductance (MscL) are affected by variations in lipid composition. Here, we utilize molecular dynamics simulations of *Mycobacterium tuberculosis* MscL to investigate such lipid composition effects on a molecular level. In particular, two sets of simulations were performed. In the first, trajectories using lipids with different headgroups (phosphatidylcholine and phosphatidylethanolamine) were compared. Protein-lipid interactions were clearly altered by the headgroup changes, leading to conformational differences in the C-terminal region of *M. tuberculosis* MscL. In the second set of simulations, lipid tails were gradually shortened, thinning the membrane over a molecular dynamics trajectory. These simulations showed evidence of hydrophobic matching between MscL and the lipid membrane, as previously proposed. For all simulations, protein-lipid interaction energies in the second transmembrane region were correlated to mutagenic data, emphasizing the importance of lipid interactions for proper MscL function.

INTRODUCTION

Mechanosensitive channels are proposed to play a central role in a variety of physiological processes, including touch, hearing, and circulation (Hamill and Martinac, 2001). The best-studied channel of this class is the bacterial mechanosensitive channel of large conductance (MscL) (Batiza et al., 1999; Spencer et al., 1999). Rees and co-workers solved a crystal structure of *Mycobacterium tuberculosis* MscL (Tb-MscL), showing the channel assembles as a homopentamer (Chang et al., 1998). In the structure, each of the channel subunits contains two transmembrane domains connected by an extracellular loop and a sizable C-terminal domain forming a helical bundle. The first transmembrane domain (TM1) lines the pore, whereas the second transmembrane domain (TM2) faces the lipid.

MscL is gated by the application of tension to the lipid bilayer (Sukharev et al., 1999), and its gating is not dependent on any other protein or cellular structure as it is fully functional when purified and reconstituted alone in lipid vesicles (Häse et al., 1995). When a bacterium experiences osmotic downshock it swells, producing a tension in the membrane. At a critical value for the tension, MscL opens, acting as a ''safety valve'' to prevent lysis (Levina et al., 1999; Nakamaru et al., 1999; Wood, 1999). The open channel is not ion-selective and can pass relatively large organic ions (Cruickshank et al., 1997), leading to a predicted pore diameter of $\approx$40 Å. Researchers have debated whether MscL can pass small proteins, such as thioredoxin and EF-Tu (Ajouz et al., 1998; Berrier et al., 2000; Vasquez-Laslop et al., 2001).

Submitted January 20, 2003, and accepted for publication April 21, 2003.

Address reprint requests to Dennis A. Dougherty, Mail Code 164-30 Cr, California Institute of Technology, Pasadena, CA 91125. Tel.: 626-395-6089; Fax: 626-564-9297; E-mail: dad@igor.caltech.edu.

0006-3495/03/09/1512/13 $2.00

It is clear that interactions between the channel and surrounding lipid are central to MscL gating. Not surprisingly, MscL gating properties are dependent on membrane lipid composition. Recent work has shown that *Escherichia coli* (Ec) MscL incorporated into lipid vesicles gates at a lower tension when the lipid tails are shortened (Kloda and Martinac, 2001; Perozo et al., 2002b). It is thought that the channel opens more easily because of better hydrophobic matching between the shorter lipid tails of the thinned membrane and the intermediate and/or open states of MscL. Such hydrophobic matching has been proposed to play a major role in channel gating, since the membrane thins upon the application of tension (Hamill and Martinac, 2001; Sukharev et al., 2001b). Other work has shown that the gating physiology of both Tb-MscL (Moe et al., 2000) and Ec-MscL (Sukharev et al., 1993) differs when the channels are expressed in spheroplasts versus being incorporated into asolectin vesicles. However, systematic studies of the effects of lipid identity and composition on MscL gating have not been reported.

Molecular dynamics (MD) simulations can give further insight into how lipid composition affects MscL structure and dynamics on the molecular level. The Tb-MscL crystal structure has provided a starting point for previous MD simulations of the channel embedded in an explicitly represented lipid membrane (Elmore and Dougherty, 2001; Gullingsrud et al., 2001). Such simulations did point to some intriguing protein-lipid interactions (Elmore and Dougherty, 2001). However, each of these previous MD studies considered only one type of lipid, palmitoyloleoyl-phosphatidylethanolamine (POPE) (Elmore and Dougherty, 2001) or palmitoyloleoylphosphatidylcholine (POPC) (Gullingsrud et al., 2001), so comparisons of the effects of different lipids in directly analogous simulations were not possible. Similarly, most MD studies of membrane proteins only consider

a single type of lipid (see Roux, 2002, and Forrest and Sansom, 2000, for recent reviews of these simulations). Recent studies have compared how different lipids affect trajectories of glycophorin (Petrache et al., 2000b) and WALP peptides (Petrache et al., 2002). In particular, Petrache and co-workers investigated the hydrophobic matching of WALP peptides in membranes with two different tail lengths (Petrache et al., 2002). As well, other MD studies have focused on characterizing protein interactions with a single type of lipid through interaction energies and changes in lipid properties (Mihailescu and Smith, 2000; Tieleman et al., 1998; Woolf, 1998; Zhu et al., 2001). Using static protein-lipid systems, other computational methods have been used to evaluate the interaction energies between proteins and lipid membranes of varying lipid composition (Arbuzova et al., 2000; Murray et al., 1998; Murray and Honig, 2002). However, these electrostatic studies are limited as they generally do not consider possible changes in protein conformation between different lipid environments.

In this work, we report MD simulations of Tb-MscL embedded in a lipid membrane, addressing the effects of lipid headgroup type and lipid tail length on MscL. In a first set of simulations, directly comparable trajectories of Tb-MscL in POPE and POPC lipid were computed. These simulations show that the structure and dynamics of the MscL channel are directly affected by changes in lipid headgroup, particularly in the C-terminal region. In the second set of simulations, lipid tails were progressively reduced in length, producing a gradual thinning of the membrane over a multinanosecond trajectory. These simulations differ from previous MD simulations of proteins that separately embedded the protein of interest into lipids with differing chain lengths (Petrache et al., 2000b, 2002). In the present study, gradual thinning could be particularly advantageous, as it may serve as a crude proxy for the application of tension to the protein-lipid system. Since possible problems in attempting to simulate MscL gating with computationally applied tension have been outlined (Bilston and Mylvaganam, 2002), our indirect approach could be particularly useful. Overall, these shortening simulations support the previously proposed hydrophobic matching of MscL. Furthermore, in light of recent extensive random mutagenesis of Ec-MscL (Maurer and Dougherty, 2003), consideration of protein-lipid and intersubunit interactions in both sets of trajectories further highlight the central importance of protein-lipid interactions to proper channel function.

METHODS

Simulation setup

The Tb-MscL crystal structure (Chang et al., 1998) with all ionizable residues charged (Asp, Glu, Lys, and Arg; no His are present in Tb-MscL) and uncharged N- and C-termini ($-NH_2$ and $-COOH$) was used as the starting structure for the channel in all simulations. The termini were left uncharged, as neither is a real protein terminus, and additional charges could cause spurious interactions. This structure was initially embedded into an equilibrated POPE membrane (Tieleman and Berendsen, 1998) as in previous Tb-MscL MD simulations (Elmore and Dougherty, 2001). Throughout, the membrane was oriented in the *xy* plane, with the *z*-axis as the membrane normal. The positioning of the channel in the normal of the membrane (the *z*-axis) was consistent with the electron paramagnetic resonance (EPR) results of (Perozo et al., 2001). Unlike our previously reported simulations, all residues in the Tb-MscL channel crystal structure (Ala10-Arg118) were included in the simulations. This was done because recent mutagenic data has begun to probe the functional and structural importance of the Tb-MscL C-terminal region (Maurer, Elmore, and Dougherty, unpublished data), despite its demonstrated unimportance in Ec-MscL (Blount et al., 1996). Overall, this system included 545 protein residues, 290 POPE lipids, and 23,523 water molecules, for a total of 90,829 atoms; the initial system size is ~9.7 nm × 9.5 nm × 12.4 nm. The full simulation system is shown in Fig. 1. This initial system was treated analogously to previous simulations, applying 150 steps of steepest descents minimization to reduce close contacts and gradually heating to 310 K over 20 ps with restraints on all Cα atoms of the channel. All subsequent simulations were performed at 310 K.

Simulations with different lipid headgroups

In the initial POPE system, the full Cα restraints were maintained after heating for 180 ps. Subsequently, they were released in gradual steps over an additional 330 ps; afterwards no restraints were placed on the system.

The headgroup change from POPE to POPC was performed at the 1000 ps frame of the POPE trajectory. This point was chosen because the membrane had been allowed to grossly adjust to the channel after embedding, but the protein structure had not fully entered into its equilibrium interactions with the lipid. At this frame, all the hydrogens attached to the *N* of the ethano-

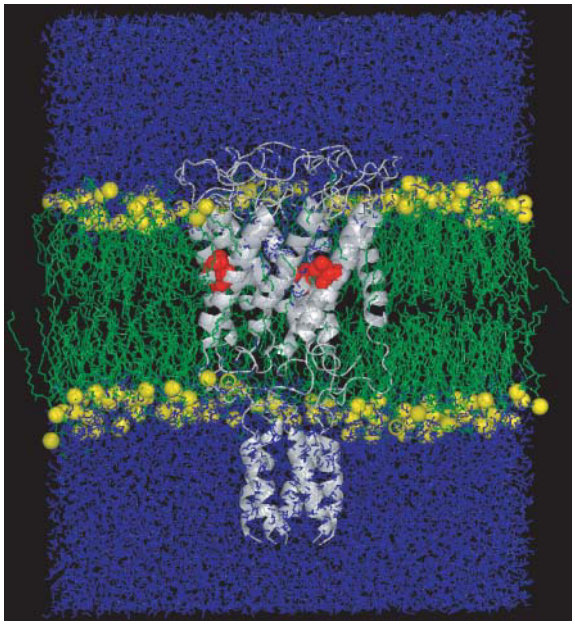

FIGURE 1 The full simulation system at the end of 100 ps of MD simulation. The channel is shown in white ribbon with residue L81, shown by EPR measurements to lie near the middle of the bilayer (Perozo et al., 2001), highlighted as red space-filling. Water is depicted as blue wireframe, and lipid molecules are green wireframe with phosphate atoms in yellow space-filling.

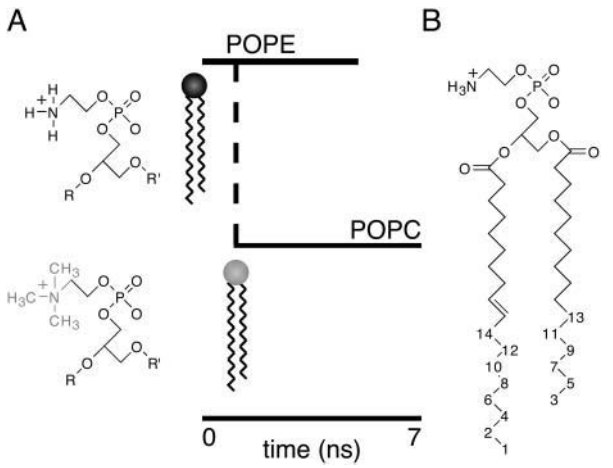

FIGURE 2 (*A*) Chemical structures of POPE and POPC headgroups are shown on the left, with the portion differing in POPC highlighted in gray. On the right is a schematic of the lipid headgroup changing simulations. In the schematic, the dashed line shows where all lipids in the 1-ns frame of the POPE trajectory were converted to POPC. (*B*) The structure of 16/18 PE showing the order in which carbons were removed from lipid tails in lipid shortening simulations. As discussed in the text, the first two carbons were removed from the oleoyl chain, after which carbons were removed from alternating chains.

lamine moiety of the POPE headgroups were changed into methyl groups (Fig. 2 *A*), and the system was subjected to 50 steps of steepest descents minimization to reduce newly introduced close contacts before extending the POPC trajectory for an additional 6 ns. The POPE trajectory was extended to a total of 5 ns.

Differences between phosphatidylethanolamine (PE) and phosphatidylcholine (PC) headgroup interactions may be due to differences in electrostatics. Recent work has advocated the use of particle mesh Ewald (PME) methods for optimal handling of long-range electrostatics in simulations of lipid bilayers and membrane proteins (Faraldo-Gómez et al., 2002; Feller et al., 1996). However, since others report that the two methods yield quite similar results for some systems (Capener and Sansom, 2002), we compared simulations of Tb-MscL in POPE that utilized either an electrostatic cutoff (1.8 nm) or PME for long-range electrostatics. The channel structures in these simulations were qualitatively similar except for the C-terminal region, which exhibited a greater deviation from the crystal structure in the cutoff simulation. Since recent experimental work has focused on this region in Tb-MscL (Maurer, Elmore, and Dougherty, unpublished data) and lipid interactions could be important in that region, we opted to use PME (Darden et al., 1993) for long-range electrostatics in POPE and POPC comparison simulations, with 1.0-nm Coulombic and Lennard-Jones cutoffs. The PME calculations utilized a Fourier grid spacing of 0.10 nm and cubic interpolation.

Simulations with lipid tail shortening

For lipid shortening simulations, full Cα restraints were applied to the heated system for 80 ps. This was followed by a gradual release of those restraints over the following 165 ps of the trajectory; no restraints were placed on the system after that point.

Lipid tail shortening simulations started from the 500-ps frame of a POPE trajectory. Shortening was done by removing the terminal methyl group of one lipid tail and equilibrating the system for 300 ps. After this equilibration time, another methyl was removed, followed by another equilibration window. The order in which carbons were removed is depicted in Fig. 2 *B*. Initially, the lipid tails were 16 (palmitoyl) and 18 (oleoyl) C atoms in length; this is denoted as 16/18 lipid throughout this article. The two terminal carbons of the 18 C chain were removed first. After this removal, the lipid was 16/16, and carbons were removed from alternating tails, beginning with the tail that was initially 16 C. In the case where the lipid was shortened to 10/10, the oleoyl double bond was converted to a single bond between the removal of C11 and C12. This was done to prevent an unsaturated unit from occurring at the end of a lipid tail, as this could lead to unusual lipid dynamics. After the lipid tails were reduced to the desired length—14/14, 12/12, or 10/10—the trajectory was extended (2 ns for 14/14 and 12/12 simulations, and 5 ns for the 10/10 simulation). Since previous embedded systems began to show equilibration of protein-lipid interactions after 1 ns (Zhu et al., 2001), these extensions allowed the system to adjust before an averaging period for analyses. The 16/18 trajectory was extended to a total of 3 ns.

To confirm that the 300-ps equilibration between shortening steps is sufficiently long, an additional shortening trajectory to 14/14 was performed using 600-ps equilibration times. This trajectory was qualitatively similar to the 300-ps step trajectory, although some details of the simulations were different. For example, the 600-ps trajectory showed somewhat less overall bilayer thinning. This might occur because the bilayer initially overcompensates after some lipid shortening events, and this slight overthinning is not fully remediated in the shorter time steps. Also, the relative sizes of the hydrophobic matching effects (border/bulk lipid thickness differences and protein hydrophobic surface length adjustment) differed between the simulations, although their total effect (defined in Eq. 1 below) was the same. Nonetheless, since both methods led to the same interpretations for the system, the more extensive 300-ps step shortening simulations will be discussed in this work.

Lennard-Jones energies and electrostatics were cut off at 1.0 nm and 1.8 nm, respectively, in these simulations. Similar cutoffs were used in previous simulations of Tb-MscL (Elmore and Dougherty, 2001) and other ion channels, such as KcsA (Shrivastava and Sansom, 2000; Shrivastava et al., 2002). Despite the possible benefits of PME methods described above, cutoffs were utilized for long-range electrostatics in these simulations to increase computational efficiency and allow consideration of a greater variety of lipid lengths and shortening protocols. Moreover, these simulations were primarily aimed at investigating the lipid-exposed TM domains, which are generally dominated by hydrophobic interactions, whereas the main differences between cutoff and PME simulations appeared to be in the C-terminal domain of the channel.

Simulation details

All minimizations and MD simulations were performed using the GROMACS 3 suite of programs (Berendsen et al., 1995; Lindahl et al., 2001). The protocols for MD used in this study were analogous to those used in our previous Tb-MscL simulations (Elmore and Dougherty, 2001). Lipid parameters were from Berger et al. (1997), with additional parameters for the oleoyl double bond taken from the GROMOS force field. GROMACS atomic parameters were used for protein and water, with some nonbonded parameters determined by standard combination rules. All MD runs used a time step of 2 fs along with the LINCS routine to constrain bond lengths (Hess et al., 1997) and SETTLE to constrain rigid water geometries (Miyamoto and Kollman, 1992). Structures from the trajectories were stored every 0.5 ps for analysis. The NPT ensemble was employed with anisotropic pressure coupling in each direction to 1 bar with a time constant (τ_p) of 1.0 ps (Berendsen et al., 1984); this coupling scheme should allow the bilayer system to properly adjust to the embedded protein and alterations in lipid composition. Temperatures were coupled separately for protein, lipid, and solvent to a temperature bath with a coupling constant (τ_t) of 0.1 ps (Berendsen et al., 1984).

Analysis of the trajectories was primarily performed with the GROMACS suite. All average properties, such as energies and distances, were computed over the final 1 ns of a particular trajectory, unless otherwise noted. Interaction energies were averaged over all saved frames, including

both short- and long-range electrostatics and Lennard-Jones energies. Due to the difficulty of calculating long-range energies between several different portions of the system with PME, per-residue long-range interaction energies were calculated with cutoffs of 2.25 nm for simulations run with PME. These energies were unaffected qualitatively by changing the cutoff value used for this analysis. The definitions of the protein regions—TM1, extracellular loop, TM2, and C-terminal—were residues 15–43, 44–68, 69–89, and 90–118, respectively, as defined previously (Maurer et al., 2000). Hydrogen bonds were defined geometrically as interactions in which the distance between the hydrogen and the acceptor is <0.25 nm and the interaction angle is $\leq 60°$; amide N atoms were omitted as possible hydrogen bond acceptors. Bordering lipids were defined as those with an average minimal distance of 0.35 nm or less from the channel, as in past Tb-MscL simulations (Elmore and Dougherty, 2001). Statistical analyses were performed using SPSS (Chicago, IL). Molecular graphics were generated with Pymol (W. L. DeLano, http://www.pymol.org).

RESULTS AND DISCUSSION

Simulations with different lipid headgroups

Overall comments

The transformation of lipid from POPE to POPC resulted in a system which adjusted and stabilized its membrane properties, such as lipid density and lipid *P-P* distance, in a few ns (data not shown). This included the expected lateral spreading of the PC membrane accompanied by an overall thinning of the bilayer. As well, the protein was generally stable throughout equilibration. The overall channel RMS deviation from the crystal structure was very similar for the first few ns after the change to POPC (Fig. 3). However, there was then a rapid transition in the RMS deviation ~2 ns after the alteration. This transition corresponded to changes in the structure of the C-terminal domain. The RMS deviations for other regions of the protein remained very similar between the trajectories and were comparable to those observed in previous Tb-MscL simulations (Elmore and Dougherty, 2001; Gullingsrud et al., 2001).

The number of protein-lipid hydrogen bonds decreased upon the change from POPE to POPC (Fig. 4). Previous simulations in POPE had shown that the lipid ethanolamine moiety was the donor in a high proportion of all MscL-lipid hydrogen bonds (Elmore and Dougherty, 2001). Since such hydrogen bond donation is not possible with POPC, the observed decrease in hydrogen bonding was expected. Diminished hydrogen bonding was most notable in the extracellular loop (Fig. 4), which after equilibration had only 40% as many hydrogen bonds in POPC as in POPE. The drop in the C-terminal region was also marked, but of a lower magnitude (69% of POPE).

Lipid-dependent conformation of the C-terminal region

The most notable effects resulting from changing the lipid headgroup from PE to PC are in the Tb-MscL C-terminal region. As discussed above, this region shows a structural transition ~2 ns after the change, resulting in greatly increased RMS deviation from the crystal structure (Fig. 3). In this transition, the upper portion of the C-terminal region appears to adjust its conformation, leading the helical regions to approach the membrane more closely (Fig. 5). The decrease in C-terminal protein-lipid hydrogen bonding interactions in POPC likely plays a role in this conformational transition. The energetic factors leading to the observed structural changes can be considered by examining protein-lipid interaction energies per residue in the two trajectories (Fig. 6 *A*). In POPC, protein-lipid interactions are markedly decreased at Y94 and E102. Without these strong interactions, the channel rearranges in POPC to make

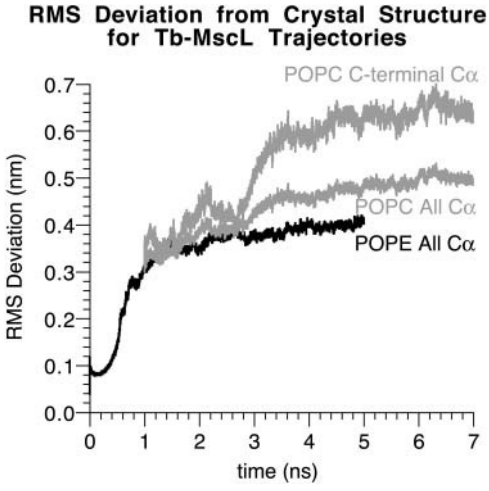

FIGURE 3 RMS deviation from crystal structure for POPE (*black*) and POPC (*gray*) trajectories. These values were calculated for each frame of the simulations by first fitting all protein Cα to the crystal structure. RMS deviations after fitting are reported for all Cα in both trajectories and for Cα in only the C-terminal region in the POPC trajectory.

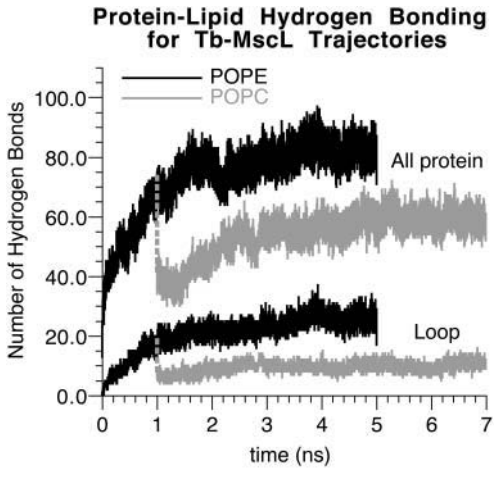

FIGURE 4 Number of hydrogen bonds between lipid and either the entire channel or only the extracellular loop in the POPE and POPC trajectories. Dashed lines show where POPE lipids were converted to POPC at 1 ns.

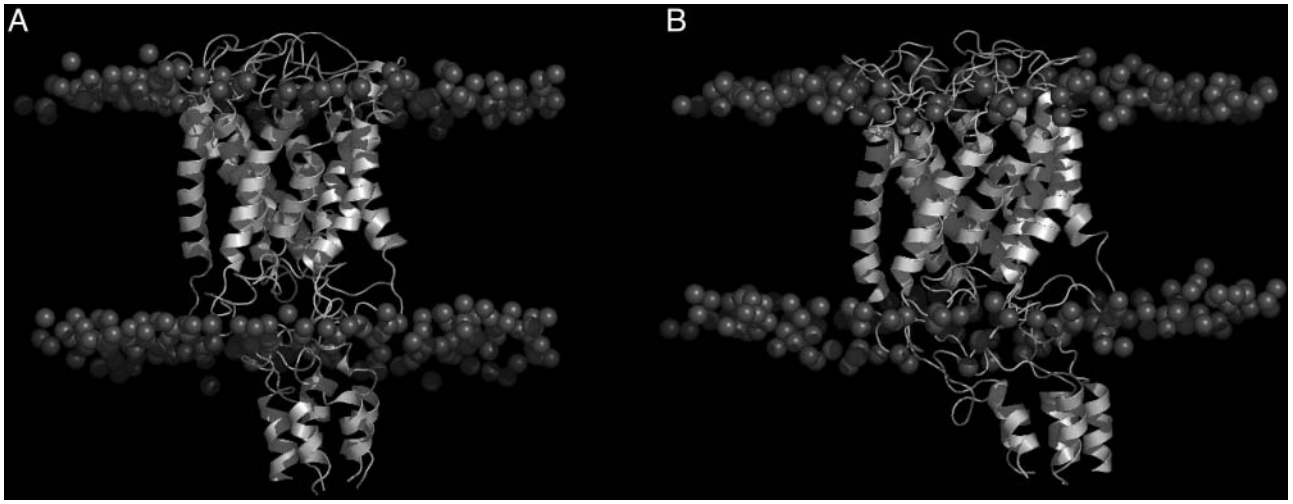

FIGURE 5 Pictures of the final frames of the POPE (*A*) and POPC (*B*) trajectories, with the protein shown as white ribbon and the lipid phosphate atoms shown as gray space-filling.

interactions at K99 and K100 more favorable. These structural changes bring the C-terminal region closer overall to the membrane (Fig. 5 *B*), increasing lipid interaction with D108 and E116 (Fig. 6 *A*). As well, these rearrangements lead to the opposite effect in intersubunit interactions at the same sites: decreased intersubunit interactions at K99 and K100 and more favorable intersubunit interactions at E102 (Fig. 6 *B*). Most of the residues showing altered lipid interactions are highly conserved among MscL orthologs (Maurer et al., 2000). K99, K100, and E102 are part of a highly charged region found in all orthologs and determined to be essential for channel function in cleavage studies of Ec-MscL (Blount et al., 1996). D108 and E116 also have acidic counterparts in other MscL channels. Thus, lipid interactions noted in these simulations may play a general role in influencing the structure and the functional role of MscL C-terminal regions.

Thus, it appears that interactions with POPE lipids can promote the crystal structure conformation of the Tb-MscL C-terminal helical domain. Recent data has shown that some single-site mutations in this region lead to altered thermal stability as determined by CD melting studies (Maurer, Elmore, and Dougherty, unpublished data). It would be particularly interesting to determine the relationship between these structural changes and Tb-MscL function. As well, the gating tension of Tb-MscL is quite high (compared to that of Ec-MscL) when expressed in *E. coli* spheroplasts (Moe et al., 2000), which have a high proportion of PE lipid (≈75%) in their inner membrane (Raetz, 1978). Conversely, *M. tuberculosis* membranes contain comparatively little PE lipid, <15% of their total lipid (Khuller et al., 1982; Lee et al., 1996). Instead, *M. tuberculosis* membranes consist primarily of glycolipids, such as phosphatidylinositol mannosides (PIMs). Although the sugars on PIMs do have hydroxyl groups that could serve as hydrogen bond donors, they would not form interactions as strong as the charged hydrogen bonds from PE headgroups. PIMs are most prevalent in the outer leaflet of the membrane, and so such interactions may be most relevant in the extracellular loop region discussed below. Interestingly, ornithine-based lipids, which contain an amine moiety and are hypothesized to be functionally interchangeable with PE lipids (Wilkinson, 1972), have been isolated from *M. tuberculosis* (Lanéelle et al., 1990); however, there is no direct evidence that ornithine lipids are located in the *M. tuberculosis* plasma membrane (Daffé and Draper, 1998). These observations lead to the intriguing idea that the difficulty of gating Tb-MscL in spheroplasts may be related to its adaptation for a different native lipid environment. Such a proposal merits further experimental consideration with electrophysiological and structural measurements.

The promotion of the crystal structure C-terminal conformation by lipid interactions may also reconcile some apparently conflicting results concerning the Tb-MscL C-terminal region. Previous MD simulations of the C-terminal region predicted that the region would only maintain its helical structure at low pH (or with neutralizing mutations; Elmore and Dougherty, 2001). Similarly, individual peptides with the sequence of the Tb-MscL C-terminal region only showed significant helicity at a low pH. However, these peptides showed significant α-helicity at physiological pH when attached to a TASP system (Kochendoerfer et al., 2002). The TASP system started at residue 102 of the C-terminal region, which means that the TASP would have imposed structural constraints in the region involved with POPE-protein interactions. Conversely, the previous MD simulations of the C-terminal region alone included no lipid and only had moderate restraints on residues 94 and 95, more N-terminal than either the TASP attachment to the peptide or some residues that appear to

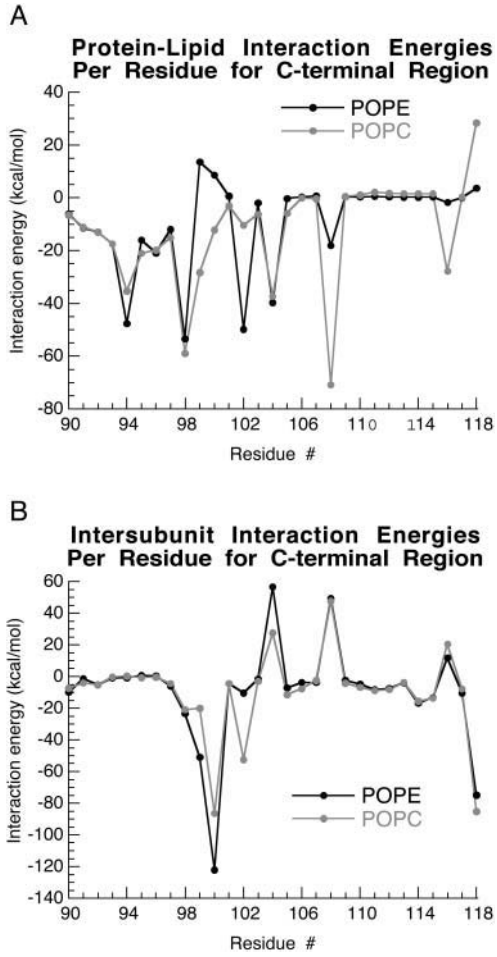

FIGURE 6 Protein-lipid (*A*) and intersubunit (*B*) interaction energies per residue for the C-terminal region in POPE (*black*) and POPC (*gray*) simulations.

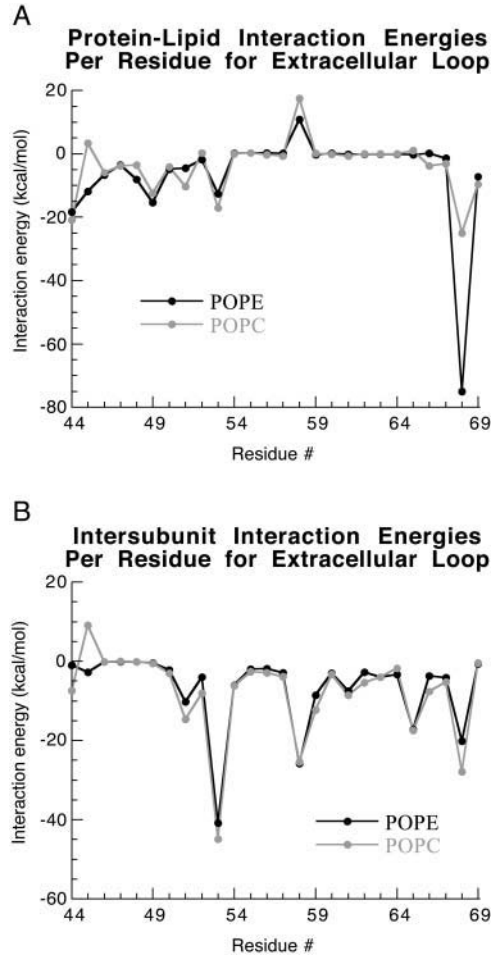

FIGURE 7 Protein-lipid (*A*) and intersubunit (*B*) interaction energies per residue for the extracellular loop region in POPE (*black*) and POPC (*gray*) simulations.

mediate important lipid interactions in our present simulations. Thus, all these studies highlight that the structure and dynamics of the C-terminal region depend on the interplay of protein-protein and protein-lipid interactions in the region directly following TM2.

Extracellular loop region

In addition to the marked decrease in hydrogen bonding described above, the protein-lipid energy profile for the extracellular loop region shows decreased interactions after the change from POPE to POPC (Fig. 7 *A*). Changes are particularly evident for two residues at the water/lipid interface, R45 and D68. Interestingly, mutagenesis at R45 has been previously shown to alter channel function, although this effect could also be due to modulation of an intersubunit hydrogen bond (Maurer et al., 2000). This drop in protein-lipid interactions does not appear to be compensated by increases in protein intersubunit interactions in POPC (Fig. 7 *B*). However, despite these energetic changes resulting from the lipid headgroup alteration, no clear structural correlates were evident in the loop region in either measurements of RMS deviation and fluctuation or by visual inspection (data not shown). Since previous work has proposed functional importance for this region in Tb-MscL (Maurer et al., 2000) and Ec-MscL (Ajouz et al., 2000), further site-specific dissection may implicate a functional importance of interactions modulated by lipid changes in this region. As well, unlike in the C-terminal region these Tb-MscL lipid interacting residues are not well-conserved among MscL orthologs outside of the Mycobacteria (Maurer et al., 2000). In fact, D68 is aligned, or closely aligned, with a positively charged K or H residue in most non-Mycobacterial channels, including Ec-MscL. These differences could be related to the known physiological differences between Tb-MscL and other MscL channels (Moe et al., 1998, 2000).

Simulations with lipid tail shortening

Overall system adjustment to lipid shortening

To simulate the bilayer thinning that accompanies a rise in tension, we progressively shortened the lipid tails by successive removals of terminal methyl groups of the lipid chains. The lipid bilayer adjusted quite rapidly to the removal of each methyl group. Bilayer thickness, measured by the distance between phosphorous atoms on opposite sides of the bilayer, decreased quickly after each shortening step and generally remained level after a few hundred ps (Fig. 8 *A*). On the average, each step thinned the membrane by 0.75–1 Å, which agrees with experimental measurements on lipid vesicle bilayers with varying tail lengths (Lewis and Engelman, 1983). In addition, the protein structure was not grossly altered in the simulations with lipid shortening, as shown by the RMS deviations between the trajectories and the starting crystal structure (Fig. 8 *B*). The RMS deviation for all Cα is relatively high in these simulations, primarily due to large deviations in the extramembrane regions. The extracellular loop was not well-ordered in the crystal structure, and the C-terminal region does not exhibit the lipid stabilization noted above when PME is not used to compute long-range electrostatics, leading to disorder similar to simulations of this region without lipid present (Elmore and Dougherty, 2001). As well, the RMS fluctuations (data not shown) of Cα atoms in equilibrated systems were essentially identical, showing no clear regions of increased or decreased structural stability in the systems with shortened lipid.

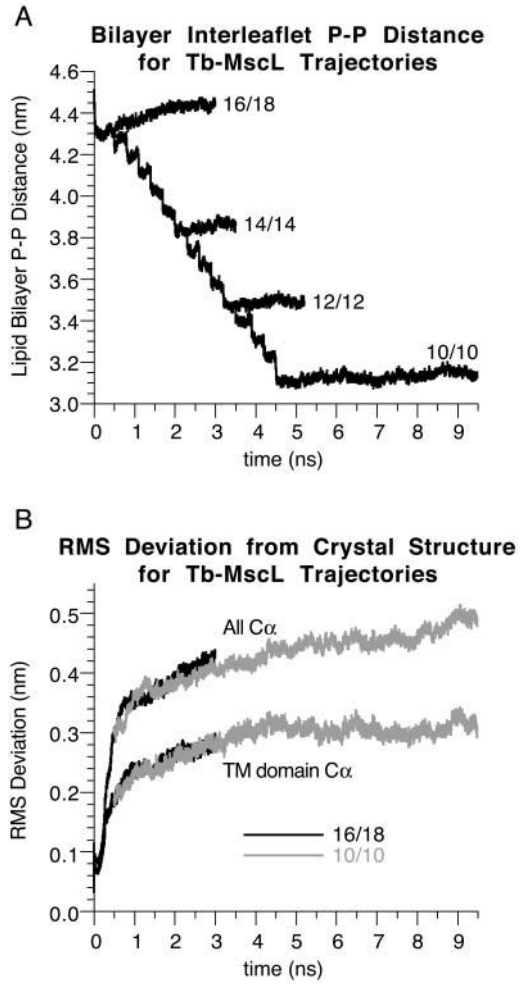

FIGURE 8 (*A*) Distance between the phosphorous atoms of the two lipid bilayer leaflets for all lipid shortening trajectories. This distance was calculated as the difference between the average *z*-axis positions of all phosphorous atoms in the leaflets. (*B*) RMS deviation from crystal structure for the trajectories ending with 16/18 lipid (*black*), and 10/10 lipid (*gray*). These values were calculated as in Fig. 3; values are reported for the RMS deviation of all Cα and just the Cα of the TM1/TM2 regions. The RMS deviation values for the trajectories ending in 14/14 and 12/12 were essentially the same as those shown.

Evidence of hydrophobic matching in the simulations

Hydrophobic matching between MscL and the surrounding lipid has been proposed as a possible driving force for channel gating (Hamill and Martinac, 2001; Sukharev et al., 2001b). Both the lipid properties and protein movements in the lipid shortening trajectories exhibit clear signs of such hydrophobic matching. First, during membrane thinning, lipids that directly border the protein thin less than lipids in the bulk of the membrane (Fig. 9). Thus, it appears that favorable interactions with the protein ''restrain'' the nearby lipids from compressing as much as those that are not directly coupled to the protein. Interestingly, in the 16/18 trajectory the opposite effect is observed, in that the bordering lipids are actually thinner than those in the bulk. This implies that the channel actually matches better to a lipid somewhat thinner than 16/18. Thus, despite the tendency of a lipid with a given tail length to form a bilayer of a particular thickness, hydrophobic matching with the channel causes lipids close to the channel to adopt a different thickness.

Changes in protein conformation in the simulations are also driven by hydrophobic matching. The majority of the channel-lipid interface consists of the second transmembrane domain and early portions of the C-terminal region. These regions can be used to define a ''hydrophobic surface'' on the outer face of Tb-MscL, as seen in Fig. 10. Although the exact definition of this surface is somewhat arbitrary, the analyses presented are robust to changing the definition by a few residues. The length of this hydrophobic surface along the bilayer normal (in the *z*-direction) decreases during the membrane thinning simulations. Fig. 10 shows this length averaged over all five subunits for trajectories with membranes of different thickness. Clearly, these surfaces attempt to compress to better match the shortened lipid.

Thus, hydrophobic matching leads to a balance between bordering lipid being restrained from full thinning and the channel decreasing its hydrophobic length. One can calculate the extent to which these combined effects compensate for

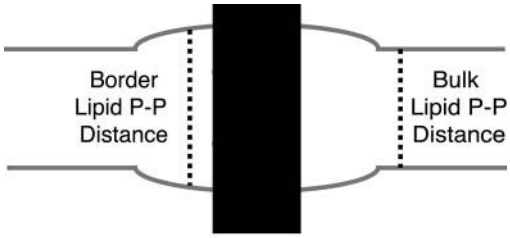

Lipid Tail	Border P-P (Å)	Bulk P-P (Å)	Δ (Border-Bulk) (Å)
16/18	43.3	44.8	-1.5
14/14	40.7	38.0	2.7
12/12	37.4	34.1	3.3
10/10	33.9	30.6	3.3

FIGURE 9 Average transbilayer distances between phosphorous atoms of lipids bordering Tb-MscL and in the bulk for lipid shortening simulations. The diagram on top schematically shows the difference between bordering and bulk lipids, with the channel depicted as a black rectangle and the lipid phosphorous atoms shown in gray. The average values for the final 1 ns of each lipid shortening simulation are given below along with the difference between values for the bordering and bulk lipids.

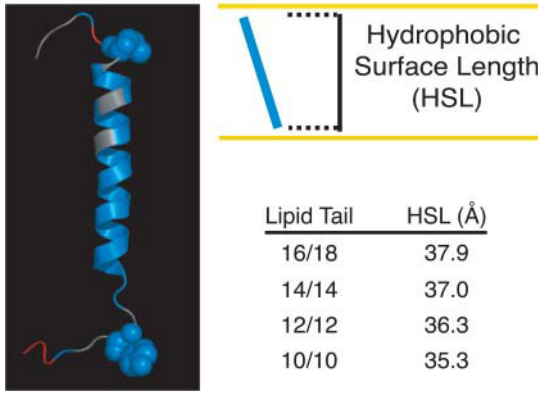

Lipid Tail	HSL (Å)
16/18	37.9
14/14	37.0
12/12	36.3
10/10	35.3

FIGURE 10 Average values for channel hydrophobic surface length (*HSL*) in lipid shortening simulations. The structure on the left denotes residues included in the ''hydrophobic surface'' of Tb-MscL, encompassing all of the TM2 helix and a portion of the C-terminus. Hydrophobic residues (Leu, Val, Ile, Ala, Phe, Tyr, and Trp) are shown in blue; charged residues (Arg, Lys, Asp, and Glu) are shown in red. The residues chosen as the termini of the ''hydrophobic surface,'' L69 and Y94, are displayed in space-filling. The diagram on the top right shows the definition of HSL for a single subunit, shown as a blue line, with the lipid phosphorous atoms denoted in yellow. Average HSL values for the final 1ns of all lipid shortening simulations are given on the bottom right.

the overall thinning of the bulk membrane from 16/18 to *X/X* using the expression:

$$\%\,compensation = \frac{border\ lipid\ effect + HSL\ effect}{total\ bulk\ lipid\ thinning} = \frac{[border\ PP(X/X) - bulk\ PP(X/X)] + [HSL(16/18) - HSL(X/X)]}{bulk\ PP(16/18)\ -\ bulk\ PP(X/X)}, \quad (1)$$

where *PP*(*X/X*) is the average interleaflet *P-P* distance for the lipid *X/X* and *HSL*(*X/X*) is the hydrophobic surface length in the lipid *X/X*. Using this expression, the hydrophobic matching effects are 40–50% of the overall bulk membrane thinning in the 14/14, 12/12, and 10/10 trajectories, with the percentage decreasing for the increasingly thinner bilayers. Thus, the system shows only a partial compensation for the thinning effects. Perhaps more extensive lipid or protein perturbations would occur on a longer simulation timescale. Also, since the percent compensation decreased with more extensive thinning, the lipid and channel may have become increasingly decoupled from one another under such extreme shortening.

A border lipid effect also was observed in the POPC simulation described above. In the bulk, POPC thins considerably compared to POPE, from 44.2 Å to 38.1 Å. This thinning is in agreement with experimental comparisons between PE and PC lipids with identical hydrocarbon tails (Petrache et al., 2000a; Rand and Parsegian, 1989). However, our magnitude of thinning is somewhat greater than the 1–4 Å observed experimentally. This may result from bulk lipids overcompensating for the lack of thinning in border lipids, which are highly restrained, maintaining a thickness of 43.2 Å. The protein HSL showed no change in POPC vs. POPE. These simulations used the PME electrostatic model, and interestingly, the thinning of the border lipids noted above for the 16/18 POPE system was not seen when PME electrostatics were used. Thus, the inverse effect seen for 16/18 border lipids may have been an artifact of the less sophisticated cutoff electrostatics. However, the POPC results confirm that hydrophobic matching upon thinning is insensitive to the electrostatic method employed.

Structural rearrangements upon bilayer thinning

The decreased average hydrophobic surface length discussed above is not a consequence of a smooth, concerted motion of the five subunits of MscL, but rather results from especially large movements in one or two of the subunits. We considered the possibility that these motions could provide

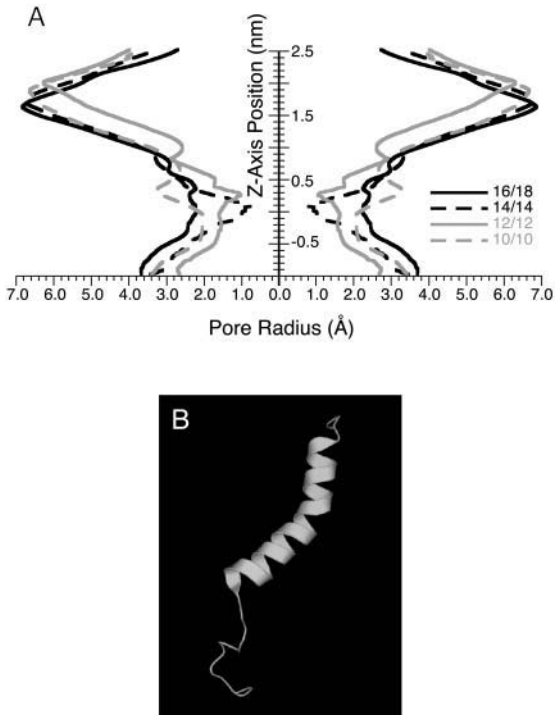

FIGURE 11 (*A*) Pore radius profiles for lipid shortening simulations calculated with HOLE (Smart et al., 1997). Frames taken every 50 ps for the final 250 ps of a trajectory were averaged for the profiles presented. The *z*-axis position of each profile was adjusted such that V21 was at 0 nm. (*B*) An example of a kinked TM2 helix from the final frame of the 10/10 trajectory.

insights into the early conformational changes of Tb-MscL resulting from membrane thinning upon the application of tension to the membrane. One feature of the simulations was that pore constrictions were observed in the 14/14 and 12/12 shortening simulations (Fig. 11 *A*). These trajectories exhibited a narrowed pore in the region near the V21 plug residue, extending to more extracellular portions of the pore.

Our MD simulations also showed changes in TM2 conformation, and these contribute to the decreased hydrophobic surface length of the channel. However, these movements were not consistent between simulations. In some cases, the hydrophobic shortening resulted from tilting and/or kinking motions of the helical TM2 region (Fig. 11 *B*). However, in other cases, thinning resulted from a compression of the less structured C-terminal portion of the hydrophobic surface. It remains to be determined whether one or both of these motions lie along the early stages of the MscL gating pathway. Further investigations of such motions, such as possible kinks in the TM2 region, would be valuable, especially since helical kinking has been proposed to be important in the gating of other ion channels (Tieleman et al., 2001).

Additionally, it is interesting to note that the channel seems to adjust its average hydrophobic length with relatively minor conformational changes. Thus, the trajectories imply that although hydrophobic matching clearly occurs between Tb-MscL and the lipid membrane, this effect alone may not be sufficient to cause the major conformational changes leading to channel gating. This view is consistent with recent experiments showing that although MscL is easier to gate in vesicles with shorter lipid tail lengths, the channels still require some additional tension or perturbation in membrane structure to actually open (Perozo et al., 2002b).

Comparisons to experimentally derived intermediate gating models

The motions observed in our lipid shortening simulations clearly do not lead to an open state of MscL. However, it is interesting to consider them in light of gating intermediates developed by Sukharev, Guy, and co-workers (Sukharev et al., 2001a,b) and Perozo, Martinac, and co-workers (Perozo et al., 2002a,b). The Sukharev/Guy intermediate model is much further along the gating pathway than any state we observe, making comparisons to it impossible. However, the relatively early Perozo/Martinac intermediate model, which was based on EPR measurements of spin-labeled MscL incorporated in thin (14/14) membranes, seems ideal for comparison. In fact, one significant feature of their model was a pore constriction analogous to that described above for the 14/14 and 12/12 trajectories (Perozo et al., 2002a). As well, this constriction was not observed for EPR measurements in the shortest lipids, similar to its disappearance upon shortening to 10/10 lipid in our simulations (Perozo et al., 2002b).

While this agreement between experiment and simulation is gratifying, another feature of the Perozo/Martinac model, a consistent TM1 rotation and tilt, was not observed in the simulations. Instead, extracellular portions of TM1 regions moved inwards toward the pore. Additionally, the Perozo/Martinac intermediate structure in 14/14 lipid does not propose any TM2 movements of the sort observed here. These differences between simulation and experiment could be a result of the relatively short timescale of these MD simulations. We note, however, that the model building used to interpret the experimental EPR was fairly simplistic, involving rigid helices and imposed fivefold symmetry (Perozo et al., 2002a). The MD simulations reported here do not involve such constraints. Regardless, the idea of a slightly constricted intermediate state is intriguing, and determining its physiological relevance, if any, warrants further effort.

Correlations between TM2 energetic profiles and mutagenic data

The protein-lipid and intersubunit interaction energy profiles for the Tb-MscL TM2 region both show distinct peaks that follow a helical pattern (Fig. 12 *A*). This pattern occurs because one face of the TM2 helix faces the lipid bilayer,

A

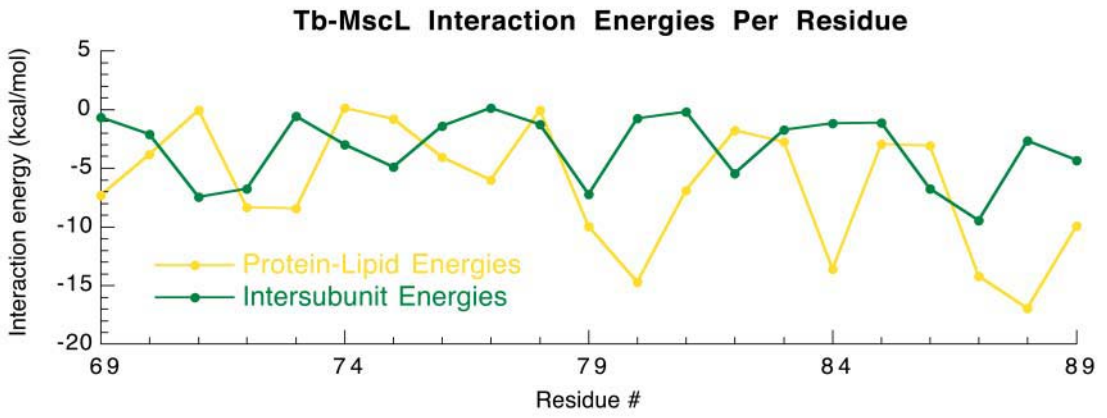

B

Tb-MscL	L69	N70	V71	L72	L73	S74	A75	A76	I77	N78	F79	F80	L81	I82	A83	F84	A85	V86	Y87	F88	L89
Ec-MscL	Y75	G76	V77	F78	I79	Q80	N81	V82	F83	D84	F85	L86	I87	V88	A89	F90	A91	I92	gap	F93	M94
Intersubunit																					
Lipid																					
LOF	D			YS	LN			D	G			P		E				F			
GOF									Y			R									
wt	C	S	AD	LI	V	R	DIS	AP	ILS	EGV	L		TVF	GL		CLSV	T	TVL		LS	

FIGURE 12 (*A*) Protein-lipid (*yellow*) and intersubunit (*green*) interaction energies per residue for the TM2 region of the POPE trajectory. Analogous profiles for the POPC and lipid shortening trajectories were essentially the same, showing identical energy peaks for protein-lipid and intersubunit energies. (*B*) The correlation between Ec-MscL random mutagenesis data (Maurer and Dougherty, 2003) and MD interaction energies. The sequence alignment for Tb-MscL and Ec-MscL in the TM2 region is given on the two top rows. Below this, residues that are peaks for protein-lipid (*yellow*) and intersubunit (*green*) interactions in MD simulations are denoted. On the bottom three rows, results from random mutagenesis are summarized, showing Ec-MscL mutations which yielded gain-of-function (*blue*), loss-of-function (*red*), and wild-type-like (*black*) phenotypes.

while another face interacts with the TM1 region of an adjacent subunit. These profiles are qualitatively unaltered by changes in lipid headgroup or lipid tail shortening.

Recent random mutagenesis studies of Ec-MscL have characterized several mutations in the TM2 region (Maurer and Dougherty, 2003). Many such mutations were determined to be gain-of-function (GOF), i.e., gating more easily than wild-type, or loss-of-function (LOF), i.e., gating with more difficulty than wild-type. Since the sequence homology between Ec-MscL and Tb-MscL is fairly high in this region (Maurer et al., 2000), we have compared this mutagenic data with our computed energetic profiles. In particular, we were interested in seeing whether residues that interact with lipid or those that interact with other subunits would be more sensitive to mutation. The experimental and computational results are summarized in Fig. 12 *B*. Strikingly, almost all mutations that lead to an altered channel phenotype occur at positions in Ec-MscL that align to lipid interacting residues in Tb-MscL; this distribution is statistically significant by Fisher's exact test ($p = 0.042$). An analogous correlation does not exist for residues that mediate intersubunit interactions ($p = 1.0$).

These results imply that lipid interactions are more important than intersubunit interactions in determining normal MscL function. Mutation of lipid interacting residues could feasibly alter channel function in at least two manners. First, these mutations could affect interactions between the channel and surrounding lipid that are necessary for the transduction of tension between the bilayer and protein. Since MscL is known to gate when reconstituted alone in lipid vesicles (Häse et al., 1995), such protein-lipid interactions must be essential to transmitting the gating tension to the channel. However, the LOF phenotype observed for many mutations at lipid interacting residues could also result from improper assembly of the channel in the membrane, since a nonfunctional channel would appear as LOF in the assay used for characterization (Maurer and Dougherty, 2001). This possibility seems most likely for mutations that would place charged or polar residues directly next to the hydrophobic membrane if MscL assembled properly; for example, Y75D. The importance of lipid interactions for proper channel assembly has been noted for other ion channels, such as KcsA (van Dalen et al., 2002).

Conversely, this analysis implies that residues which mediate MscL intersubunit interactions can be altered more readily without greatly affecting channel function. This may result from a redundancy in these interactions. There are several pairs of TM1-TM2 interactions that likely help transduce bilayer forces between the TM domains to gate the channel (Sukharev et al., 2001b), so other interactions may be able to compensate for the loss from a single mutation.

CONCLUSIONS

Considering multiple lipid environments in MD simulations of MscL has lead to insights into protein-lipid interactions that help interpret previous experiments and propose future work. Although not currently standard practice, similar consideration of multiple types of membrane may also yield interesting results for other membrane protein simulations. Certainly, the methods employed here could undergo further optimization, such as considering the effect of employing PME electrostatics in shortening simulations or extending simulations further. However, the systems were stable under our current protocols and adjusted quite quickly to the changes in lipid molecules.

In simulations comparing Tb-MscL in POPE and POPC lipids, POPE clearly seems to promote a C-terminal structure closer to the crystal structure conformation than that seen in POPC. Such differences in conformation could be one manner in which lipid composition affects Tb-MscL physiology. As well, lipid interactions and hydrogen bonding profiles were different for POPE and POPC in the extracellular loop region, although these differences did not correlate with clear structural changes in the simulations. Further experiments focusing on this region of the channel may clarify the importance of any such changes. Theoretical consideration of MscL in other types of lipid molecules using MD or other methods may lead to additional insights.

Trajectories in which lipid was gradually shortened showed that MscL does exhibit notable hydrophobic matching with lipid. Although these simulations did not lead to an open state of MscL—which would be shocking in the timescales considered—they did yield some hints of how the channel may adjust to membrane thinning. Such motions included constriction of the pore, which has also been observed experimentally (Perozo et al., 2002a), and kinking of TM helices. However, it is also interesting to note that hydrophobic matching alone may only cause relatively small changes in channel structure, which would agree with data showing shorter lipids promote channel gating but are insufficient to induce channel gating by themselves (Perozo et al., 2002b).

Protein-lipid interactions in the TM2 region of MscL also showed intriguing correlations with experimental mutagenesis data (Maurer and Dougherty, 2003). In particular, residues that were seen in MD simulations to mediate protein-lipid interactions were mutagenically more sensitive than residues that mediated intersubunit interactions within the channel. This implies that protein-lipid interactions may be more important than protein-protein interactions for proper MscL assembly and function. It will be interesting to consider if this is a general theme for mechanosensitive membrane proteins.

Overall, this work has begun to give some molecular insight into how lipid composition affects MscL structure and function. The importance of lipid interactions in MscL gating has been discussed in efforts to develop gating models of MscL, but it has been difficult to address such interactions directly in these models (Sukharev et al., 2001b). Hopefully, combinations of experiments and theoretical methods, such as those employed here, will be fruitful in developing an increasingly complete picture of the interplay between protein and membrane in mechanosensitive channel gating, and membrane protein function in general.

We are grateful to Joshua Maurer and the rest of the Dougherty Group for their thoughtful comments and suggestions, as well as to Prof. Henry Lester, Prof. Douglas Rees, and Dr. Gerd Kochendoerfer for additional discussions. A preequilibrated POPE membrane was generously made available by Prof. D. P. Tieleman.

This work was supported by National Institutes of Health program project grant GM62532.

REFERENCES

Ajouz, B., C. Berrier, M. Besnard, B. Martinac, and A. Ghazi. 2000. Contributions of the different extramembranous domains of the mechanosensitive ion channel MscL to its response to membrane tension. *J. Biol. Chem.* 275:1015–1022.

Ajouz, B., C. Berrier, A. Garrigues, M. Besnard, and A. Ghazi. 1998. Release of thioredoxin via the mechanosensitive channel MscL during osmotic downshock of *Escherichia coli* cells. *J. Biol. Chem.* 273:26670–26674.

Arbuzova, A., L. Wang, J. Wang, G. Hangyás-Mihályné, D. Murray, B. Honig, and S. McLaughlin. 2000. Membrane binding of peptides containing both basic and aromatic residues. Experimental studies with peptides corresponding to the scaffolding region of caveolin and the effector region of MARCKS. *Biochemistry.* 39:10330–10339.

Batiza, A. F., I. Rayment, and C. Kung. 1999. Channel gate! Tension, leak, and disclosure. *Structure.* 7:R99–R103.

Berendsen, H. J. C., J. P. M. Postma, W. F. van Gunsteren, A. DiNola, and J. R. Haak. 1984. Molecular dynamics with coupling to an external bath. *J. Chem. Phys.* 81:3684–3690.

Berendsen, H. J. C., D. van der Spoel, and R. van Drunen. 1995. GROMACS: a message-passing parallel molecular dynamics implementation. *Comp. Phys. Comm.* 91:43–56.

Berger, O., O. Edholm, and F. Jähnig. 1997. Molecular dynamics simulations of a fluid bilayer of dipalmitoylphosphatidylcholine at full hydration, constant pressure, and constant temperature. *Biophys. J.* 72: 2002–2013.

Berrier, C., A. Garrigues, G. Richarme, and A. Ghazi. 2000. Elongation factor Tu and DnaK are transferred from the cytoplasm to the periplasm of *Escherichia coli* during osmotic downshock presumably via the mechanosensitive channel MscL. *J. Bacteriol.* 182:248–251.

Bilston, L. E., and K. Mylvaganam. 2002. Molecular simulations of the large conductance mechanosensitive (MscL) channel under mechanical loading. *FEBS Lett.* 512:185–190.

Blount, P., S. I. Sukharev, M. J. Schroeder, S. K. Nagle, and C. Kung. 1996. Single residue substitutions that change the gating properties of a mechanosensitive channel in *Escherichia coli*. *Proc. Natl. Acad. Sci. USA.* 93:11652–11657.

Capener, C. E., and M. S. P. Sansom. 2002. Molecular dynamics simulations of a K channel model: sensitivity to changes in ions, waters, and membrane environment. *J. Phys. Chem. B.* 106:4545–4551.

Chang, G., R. H. Spencer, A. T. Lee, M. T. Barclay, and D. C. Rees. 1998. Structure of the MscL homolog from *Mycobacterium tuberculosis*: a gated mechanosensitive ion channel. *Science.* 282:2220–2226.

Cruickshank, C. C., R. F. Minchin, A. C. LeDain, and B. Martinac. 1997. Estimation of the pore size of the large-conductance mechanosensitive ion channel of *Escherichia coli*. *Biophys. J.* 73:1925–1931.

Daffé, M., and P. Draper. 1998. The envelope layers of mycobacteria with reference to their pathogenicity. *Adv. Microb. Physiol.* 39:131–203.

Darden, T. D., D. York, and L. Pedersen. 1993. Particle mesh Ewald: an N log(N) method for Ewald sums in large systems. *J. Chem. Phys.* 98: 10089–10092.

Elmore, D. E., and D. A. Dougherty. 2001. Molecular dynamics simulations of wild-type and mutant forms of the *Mycobacterium tuberculosis* MscL channel. *Biophys. J.* 81:1345–1359.

Faraldo-Gómez, J. D., G. R. Smith, and M. S. P. Sansom. 2002. Setting up and optimization of membrane protein simulations. *Eur. Biophys. J.* 31: 217–227.

Feller, S. E., R. W. Pastor, A. Rojnuckarin, S. Bogusz, and B. R. Brooks. 1996. Effect of electrostatic force truncation on interfacial and transport properties of water. *J. Phys. Chem.* 100:17011–17020.

Forrest, L. R., and M. S. P. Sansom. 2000. Membrane simulations: bigger and better? *Curr. Opin. Struct. Biol.* 10:174–181.

Gullingsrud, J., D. Kosztin, and K. Schulten. 2001. Structural determinants of MscL gating studied by molecular dynamics simulations. *Biophys. J.* 80:2074–2081.

Hamill, O. P., and B. Martinac. 2001. Molecular basis of mechanotransduction in living cells. *Physiol. Rev.* 81:685–740.

Häse, C. C., A. C. Le Dain, and B. Martinac. 1995. Purification and functional reconstitution of the recombinant large mechanosensitive ion channel (MscL) of *Escherichia coli*. *J. Biol. Chem.* 270:18329–18334.

Hess, B., H. Bekker, H. J. C. Berendsen, and J. G. E. M. Fraaije. 1997. LINCS: a linear constraint solver for molecular simulations. *J. Comp. Chem.* 18:1463–1472.

Khuller, G. K., R. Taneja, S. Kaur, and J. N. Verma. 1982. Lipid composition and virulence of *Mycobacterium tuberculosis* H37rv. *Aust. J. Exp. Biol. Med. Sci.* 60:541–547.

Kloda, A., and B. Martinac. 2001. Mechanosensitive channel of *Thermoplasma*, the cell wall-less archaea: cloning and molecular characterization. *Cell Biochem. Biophys.* 34:321–347.

Kochendoerfer, G. G., J. M. Tack, and S. Cressman. 2002. Total chemical synthesis of a 27 kDa TASP protein derived from the MscL ion channel of *M. tuberculosis* by ketoxime-forming ligation. *Bioconjugate Chem.* 13:474–480.

Lanéelle, M. A., D. Promé, G. Lanéelle, and J. C. Promé. 1990. Ornithine lipid of *Mycobacterium tuberculosis*: its distribution in some slow-growing and fast-growing mycobacteria. *J. Gen. Microbiol.* 136:773–778.

Lee, R. E., P. J. Brennan, and G. S. Besra. 1996. *Mycobacterium tuberculosis* cell envelope. *Curr. Top. Microbiol. Immunol.* 215:1–27.

Levina, N., S. Tötemeyer, N. R. Stokes, P. Louis, M. A. Jones, and I. R. Booth. 1999. Protection of *Escherichia coli* cells against extreme turgor by activation of MscS and MscL mechanosensitive channels: identification of genes required for MscS activity. *EMBO J.* 18:1730–1737.

Lewis, B. A., and D. M. Engelman. 1983. Lipid bilayer thickness varies linearly with acyl chain length in fluid phosphatidylcholine vesicles. *J. Mol. Biol.* 166:211–217.

Lindahl, E., B. Hess, and D. van der Spoel. 2001. GROMACS 3.0: a package for molecular simulation and trajectory analysis. *J. Mol. Mod.* 7:306–317.

Maurer, J. A., and D. A. Dougherty. 2001. A high-throughput screen for MscL channel activity and mutational phenotyping. *Biochim. Biophys. Acta.* 1514:165–169.

Maurer, J. A., and D. A. Dougherty. 2003. Generation and evaluation of a large mutational library from the *E. coli* mechanosensitive channel of large conductance, MscL. Implications for channel gating and evolutionary design. *J. Biol. Chem.* 278:21076–21082

Maurer, J. A., D. E. Elmore, H. A. Lester, and D. A. Dougherty. 2000. Comparing and contrasting *Escherichia coli* and *Mycobacterium tuberculosis* mechanosensitive channels (MscL): new gain of function mutations in the loop region. *J. Biol. Chem.* 275:22238–22244.

Mihailescu, D., and J. C. Smith. 2000. Atomic detail peptide-membrane interactions: molecular dynamics simulation of gramicidin S in a DMPC bilayer. *Biophys. J.* 79:1718–1730.

Miyamoto, S., and P. A. Kollman. 1992. SETTLE: an analytical version of the SHAKE and RATTLE algorithms for rigid water models. *J. Comp. Chem.* 13:952–962.

Moe, P. C., P. Blount, and C. Kung. 1998. Functional and structural conservation in the mechanosensitive channel MscL implicates elements crucial for mechanosensation. *Mol. Microbiol.* 28:583–592.

Moe, P. C., G. Levin, and P. Blount. 2000. Correlating a protein structure with function of a bacterial mechanosensitive channel. *J. Biol. Chem.* 275:31121–31127.

Murray, D., L. Hermida-Matsumoto, C. A. Buser, J. Tsang, C. T. Sigal, N. Ben-Tal, B. Honig, M. D. Resh, and S. McLaughlin. 1998. Electrostatics and the membrane association of Src: theory and experiment. *Biochemistry.* 37:2145–2159.

Murray, D., and B. Honig. 2002. Electrostatic control of the membrane targeting of C2 domains. *Mol. Cell.* 9:145–154.

Nakamaru, Y., Y. Takahashi, T. Unemoto, and T. Nakamura. 1999. Mechanosensitive channel functions to alleviate the cell lysis of marine bacterium, *Vibrio alginolyticus*, by osmotic downshock. *FEBS Lett.* 444:170–172.

Perozo, E., D. M. Cortes, P. Sompornpisut, A. Kloda, and B. Martinac. 2002a. Open channel structure of MscL and the gating mechanism of mechanosensitive channels. *Nature.* 418:942–948.

Perozo, E., A. Kloda, D. M. Cortes, and B. Martinac. 2001. Site-directed spin-labeling analysis of reconstituted MscL in the closed state. *J. Gen. Physiol.* 118:193–205.

Perozo, E., A. Kloda, D. M. Cortes, and B. Martinac. 2002b. Physical principles underlying the transduction of bilayer deformation forces during mechanosensitive channel gating. *Nat. Struct. Biol.* 9: 696–703.

Petrache, H. I., S. W. Dodd, and M. F. Brown. 2000a. Area per lipid and acyl length distributions in fluid phosphatidylcholines determined by H-2 NMR spectroscopy. *Biophys. J.* 79:3172–3192.

Petrache, H. I., A. Grossfield, K. R. MacKenzie, D. M. Engelman, and T. B. Woolf. 2000b. Modulation of glycophorin A transmembrane helix interactions by lipid bilayers: molecular dynamics calculations. *J. Mol. Biol.* 302:727–746.

Petrache, H. I., D. M. Zuckerman, J. N. Sachs, J. A. Killian, R. E. I. Koeppe, and T. B. Woolf. 2002. Hydrophobic matching mechanism investigated by molecular dynamics simulations. *Langmuir.* 18:1340–1351.

Raetz, C. R. 1978. Enzymology, genetics, and regulation of membrane phospholipid synthesis in *Escherichia coli*. *Microbiol. Rev.* 42:614–659.

Rand, R. P., and V. A. Parsegian. 1989. Hydration forces between phospholipid bilayers. *Biochim. Biophys. Acta.* 988:351–376.

Roux, B. 2002. Theoretical and computational models of ion channels. *Curr. Opin. Struct. Biol.* 12:182–189.

Shrivastava, I. H., and M. S. P. Sansom. 2000. Simulations of ion permeation through a potassium channel: molecular dynamics of KcsA in a phospholipid bilayer. *Biophys. J.* 78:557–570.

Shrivastava, I. H., D. P. Tieleman, P. C. Biggin, and M. S. P. Sansom. 2002. K^+ versus Na^+ ions in a K channel selectivity filter: a simulation study. *Biophys. J.* 83:633–645.

Smart, O. S., J. Breed, G. R. Smith, and M. S. P. Samson. 1997. A novel method for structure-based predictions of ion channel conductance properties. *Biophys. J.* 72:1109–1126.

Spencer, R. H., G. Chang, and D. C. Rees. 1999. ''Feeling the pressure'': structural insights into a gated mechanosensitive channel. *Curr. Opin. Struct. Biol.* 9:448–454.

Sukharev, S., M. Betanzos, C.-S. Chiang, and H. R. Guy. 2001a. The gating mechanism of the large mechanosensitive channel MscL. *Nature.* 409:720–724.

Sukharev, S., S. R. Durell, and H. R. Guy. 2001b. Structural models of the MscL gating mechanism. *Biophys. J.* 81:917–936.

Sukharev, S. I., B. Martinac, V. Y. Arshavsky, and C. Kung. 1993. Two types of mechanosensitive channels in the *Escherichia coli* cell-envelope—solubilization and functional reconstitution. *Biophys. J.* 65: 177–183.

Sukharev, S. I., W. J. Sigurdson, C. Kung, and F. Sachs. 1999. Energetic and spatial parameters for gating of the bacterial large conductance mechanosensitive channel, MscL. *J. Gen. Physiol.* 113:525–539.

Tieleman, D. P., and H. J. C. Berendsen. 1998. A molecular dynamics study of the pores formed by *Escherichia coli* OmpF porin in a fully hydrated palmitoyloleoylphosphatidylcholine bilayer. *Biophys. J.* 74:2786–2801.

Tieleman, D. P., L. R. Forrest, M. S. P. Sansom, and H. J. C. Berendsen. 1998. Lipid properties and the orientation of aromatic residues in OmpF, influenza M2, and alamethicin systems: molecular dynamics simulations. *Biochemistry.* 37:17554–17561.

Tieleman, D. P., I. H. Shrivastava, M. R. Ulmschneider, and M. S. P. Sansom. 2001. Proline-induced hinges in transmembrane helices: possible roles in ion channel gating. *Prot. Struct. Funct. Gen.* 44:63–72.

van Dalen, A., S. Hegger, J. A. Killian, and B. de Kruijff. 2002. Influence of lipids on membrane assembly and stability of the potassium channel KcsA. *FEBS Lett.* 525:33–38.

Vasquez-Laslop, N., H. Lee, R. Hu, and A. A. Neyfakh. 2001. Molecular sieve mechanism of selective release of cytoplasmic proteins by osmotically shocked *Escherichia coli*. *J. Bacteriol.* 183:2399–2404.

Wilkinson, S. G. 1972. Composition and structure of ornithine-containing lipid from *Pseudomonas rubescens*. *Biochim. Biophys. Acta.* 270:1–17.

Wood, J. M. 1999. Osmosensing by bacteria: signals and membrane-based sensors. *Microbiol. Mol. Biol. Rev.* 63:230–262.

Woolf, T. B. 1998. Molecular dynamics simulations of individual α-helices of bacteriorhodopsin in dimyristoylphosphatidylcholine. II. Interaction energy analysis. *Biophys. J.* 74:115–131.

Zhu, F., E. Tajkhorshid, and K. Schulten. 2001. Molecular dynamics study of aquaporin-1 water channel in a lipid bilayer. *FEBS Lett.* 504:212–218.